Table 1. Values for gases in water calculated for conditions at the surface and for a depth of 10 km, on the assumption that both the concentration and partial pressure are affected by depth.

Gas	Partial pressure of gas (atm)		M/partial molal volume (mole/ml)	Relative concentration of gas		Partial pressure of gas in water at a depth of 10 km (atm)
	At surface	At 10 km		At surface	At 10 km	
He	1.0	1.17	4/29.7	1.0	0.35	1.4
O_2	1.0	3.55	32/32	1.0	1.0	4.0
CO_2	1.0	5.7	44/34.8	1.0	1.39	5.7

justs until the force of diffusion tending to equalize the chemical potential (but not the partial pressure) is just balanced by the force of gravity. In water, the partial pressure is a function not only of the concentration but also of the buoyancy of the gas. For He the diffusion is downward, but the gravity factor is upward, whereas the reverse is true of CO_2. For O_2 there is no buoyancy factor because M is 32 and the partial molal volume is 32 ml/mole. In thermodynamics the molar free energy or the chemical potential for any gas is constant at complete equilibrium at all depths, but the total chemical potential becomes the sum of two terms, one of which is the work done against gravity (as by He) and the other is the work done on the gas by gravity (as on CO_2). Thus the total chemical potential is

$$\mu = \mu' + M\psi \tag{3}$$

where μ' is the chemical potential and $M\psi$ is the potential of the gravitational field.

These considerations lead one to the conclusion that the theoretical Teflon tube experiment permits one to calculate the partial pressure of any gas in water at any depth (Table 1). If so, then the chemical potential must also be the same at depth in the Teflon tube and in the water. Likewise, this relation ought to be true for any fluid. In every field there will be a certain solubility, partial molal volume of the gas, and density of the fluid for a given temperature, but somehow all these varying factors must balance out to give the same partial pressure of the gas that one calculates for a gas-filled tube with a membrane permeable only to that one gas. Such a tube is approximated by a Teflon tube when only one gas is present. Permeability to water might be a complicating factor, and for this reason it is assumed in theory that the membrane is permeable only to the single gas in question. It seems a rather large order to expect that such a "theoretical" Teflon tube could reach equilibrium with the same gas in any other fluid in much less than 10^6 years and a depth of 10^6 cm, but otherwise it would seem possible to use this experiment for a perpetual motion machine.

What is needed is a rigid thermodynamic proof that the partial pressure in the water at a given depth is actually equal to the partial pressure in the gas-filled Teflon tube. If this were not true, there could be diffusion of the gas either into the water or out and this would constitute perpetual motion. I have seen a proof of this kind provided by thermodynamicists whom I have consulted, and there have been many, including Klotz, whose equation was used above.

I would like to know what happens outside the Teflon tube to "tell" the water molecules how much harder they will have to "squeeze" the O_2 to prevent the O_2 in the tube from diffusing into that long fanciful reservoir of oxygenated water. Actually, the water would have to act on the few O_2 molecules so that their partial pressure increases exponentially from its sea-level value (without any change in O_2 molarity). In the O_2 tube the process is well known, and the pressure increases because there is an increasingly higher pressure of O_2 pushing down from above. The O_2 in the O_2 tube is compressed but the O_2 in the main tube outside the Teflon tube is in a nearly incompressible watery medium, and I do not clearly understand the mechanism required to bring about the necessary rise in the partial pressure of the O_2. Nor do I clearly understand why the effect of pressure is exponential and not linear.

WALLACE O. FENN*
Department of Physiology, University of Rochester School of Medicine and Dentistry, Rochester, New York 14620

References

1. T. Enns, P. F. Scholander, E. D. Bradstreet, *J. Phys. Chem.* **69**, 389 (1965).
2. T. Enns, personal communication.
3. I. M. Klotz, *Limnol. Oceanogr.* **8**, 149 (1963).

* The author died on 20 September 1971.

17 January 1972

Lunar Crust: Structure and Composition

Abstract. *Lunar seismic data from artificial impacts recorded at three Apollo seismometers are interpreted to determine the structure of the moon's interior to a depth of about 100 kilometers. In the Fra Mauro region of Oceanus Procellarum, the moon has a layered crust 65 kilometers thick. The seismic velocities in the upper 25 kilometers are consistent with those in lunar basalts. Between 25 and 65 kilometers, the nearly constant velocity (6.8 kilometers per second) corresponds to velocities in gabbroic and anorthositic rocks. The apparent velocity is high (about 9 kilometers per second) in the lunar mantle immediately below the crust.*

With the successful recording of impacts of the lunar module (LM) ascent stage and Saturn (S-IV B) rocket by the Apollo 12, Apollo 14, and Apollo 15 seismometers, discrete seismic phases that can be interpreted in terms of a velocity structure inside the moon have become available. Travel times, amplitudes, and wave shapes of compressional (P) waves have been obtained for distances from source to receiver between $\Delta = 67$ km and $\Delta = 357$ km. These data are inverted to determine the seismic velocity structure in the outer 100 km of the lunar interior. In this report we briefly describe the data, the inversion techniques, and the velocity model and its compositional significance in the light of laboratory measurements of velocities characteristic of lunar and terrestrial rocks.

Data used in the study of the earth's interior have come from a large number of earthquakes of all magnitudes and from numerous artificial sources (such as underground nuclear explosions) and have been recorded at more than a thousand seismic stations. In the case of the moon the natural seismicity (the number and energy of moonquakes) is many orders of magnitude lower than that of the earth (*1*). With only three stations it is not possible at this stage to specify the epicenter coordinates, focal depth, and time of origin of these events with sufficient accuracy to use them in structural studies. It has not been possible to detect long-period surface waves or free oscillations of the moon from such small moonquakes. Thus, we must rely on P waves from six artificial impacts, as recorded by three seismometers, for the study of the lunar interior.

The locations of the three operating stations and the impact points and wave paths are shown in Fig. 1. In their general characteristics all impact signals are similar. They are extremely prolonged with gradual buildup of the signal and long exponential decay of the signal intensity. Typically, the duration of the signals is about 2 hours. These characteristics, which are believed to be caused by intensive scattering, have been discussed (*2*) and will not be treated here. The signals corresponding to the arrival of discrete seismic phases can be identified in the early parts of the records. These are of most interest for our study.

The initial portions of the impact seismograms are shown in Fig. 2. In order to understand this figure, it is important to keep in mind that the S-IV B impact precedes the lunar landing and thus is recorded by stations operating prior to the landing. The impact of the LM ascent stage, which occurs after the lunar landed mission is completed, can be recorded with the instrument of the same mission. Furthermore, the kinetic energy of a typical S-IV B impact is about 13 times larger than that of a typical LM impact. Hence, the signals generated by S-IV B impacts have larger amplitudes than those generated by LM impacts. A change in the signal characteristics from one record to another at different distances such as $\Delta = 135$, 172, and 357 km, is also observed.

The travel times of first arrivals provide the most direct means of looking at the lunar interior. For P waves times are read from high-pass filtered or unfiltered traces. Positive identification of the signal is made by the linear polarization of the particle motion. The curve for travel time plotted against distance shown in Fig. 3a is a composite of data for first arrival P waves and later phases (surface-reflected PP and PPP). Since both source and receiver are at the surface of the moon, for phases such as PP and PPP the times can be plotted at equivalent distances (one-half and one-third the distances for first arrivals, respectively). The overall characteristics of the travel times indicate rapidly increasing velocities near the surface. An intermediate zone in which the velocity is nearly constant and a high-velocity zone below this are indicated by the two branches of the travel time curve between 186 and 357 km. In addition to these, later arrivals observed at 186 and 357 km indicate the presence of very high velocity gradients or discontinuities inside the moon.

The amplitudes (Fig. 3b) provide further evidence for velocity discontinuities. Because the geometric focusing, defocusing, and reflection of seismic rays are controlled by the velocity gradients (see ray paths in Fig. 3c), the amplitudes are sensitive indicators of rapid velocity variations. The data in Fig. 3 come from both the LM and S-IV B impact records. Since the sources have different energies, the amplitudes need to be scaled. We chose an empirical approach for this purpose and required a smooth transition from LM signal amplitudes to S-IV B signal amplitudes as a function of distance. This required a correction (multiplication) factor of 20 for LM amplitudes, a value larger than the square root of the energy ratios. However, since the angles of impact (about 3° from the horizontal for the LM and 62° or greater for the S-IV B) and the sizes of the impacting objects were different, it is reasonable to assume that S-IV B impacts would be more efficient generators of seismic waves at frequencies below 1 hz. The agreement between the theoretical curves and the observed amplitude and travel time data is good.

A more definitive approach to interpreting the lunar seismograms is to compute their theoretical equivalents (*3*). This requires, in addition to the velocity structure inside the moon, knowledge of the seismic source pulse due to the impact and the exact impulse response of the seismometer emplaced at the surface on a very low velocity regolith complex. To isolate the effect of the velocity structure, one must keep the other variables fixed. We chose the three S-IV B impact seismograms recorded at the Apollo 12

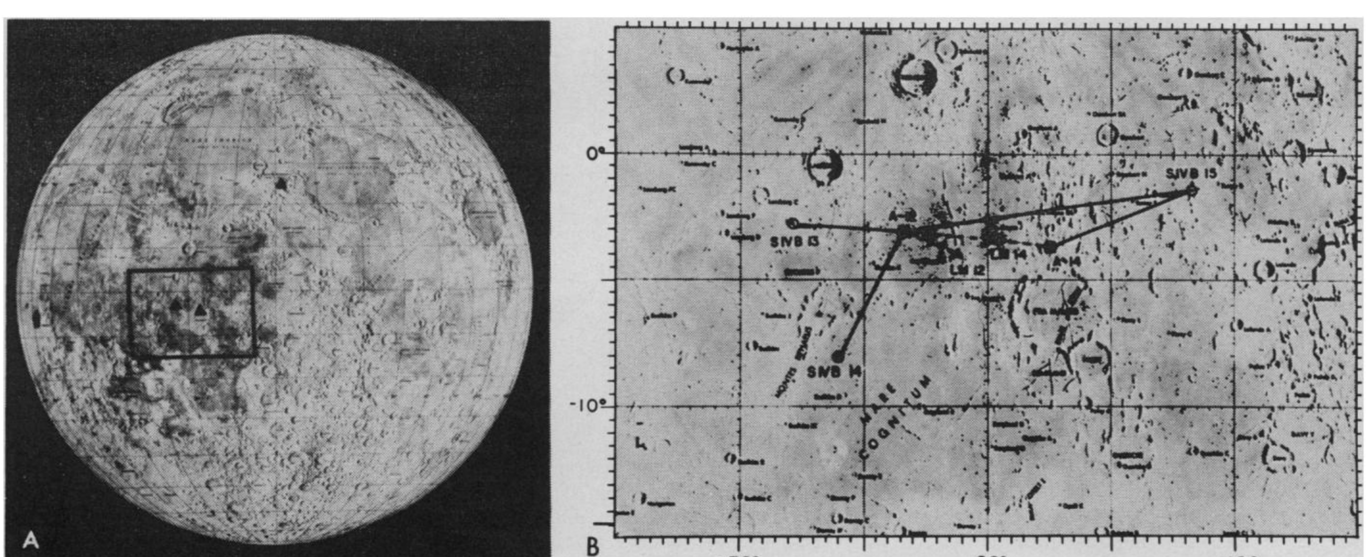

Fig. 1. (A) Location map showing the region (in frame) of the moon where most of the seismic observations have been made. Three operating seismic stations are shown as black triangles. (B) Enlarged picture showing the Apollo 12 and Apollo 14 seismic stations, the impact points, and the seismic ray paths.

station. This had the advantage of keeping the instrument response fixed while the distance from source to receiver increased for three nearly identical impacts. Because of the low signal-to-noise ratios, LM impact seismograms were excluded from matching.

The observed and computed seismograms at distances $\Delta = 135$, 172, and 357 km are shown in Fig. 4. The source function was chosen such that at 172 km the seismograms were matched exactly for the first 8 seconds. The general characteristics of the observed seismograms change significantly from 135 to 172 km and again from 172 to 357 km. These are matched closely by the theoretical seismograms.

The velocity model finalized on the basis of the fit to the travel times, amplitudes, and synthetic seismograms is shown in Fig. 5a. The main features of the velocity profile are:

1) Very rapid increase at very shallow depths from 0.1 km/sec (*4*) at the surface to about 5 km/sec at a depth of 10 km. The details of the model and whether the velocities increase smoothly or stepwise in the upper 5 km cannot be resolved without additional data at distances (Δ) closer than 30 km.

2) A sharp increase (discontinuity) at a depth of about 25 km.

3) A nearly constant value (about 6.8 km/sec) between 25 and 65 km.

4) A significant and discontinuous increase at the base of the lunar crust (65 km).

5) As determined from a single data point correspondng to $\Delta = 357$ km, very high apparent velocity (greater than 9 km/sec) below the lunar crust.

From comparisons with the velocities characteristic of the earth's crust and mantle, it is appropriate to define the base of the "lunar crust" at the discontinuity at 65 km. Although this is greater than the average thickness of the earth's crust, the jump of the velocity at this interface from about 7.0 to 9.0 km/sec is similar to the increase at the Mohorovicic discontinuity. If hydrostatic pressure instead of depth is used as the variable, the base of the lunar crust occurs at a pressure of 3.5 kbar, which is reached at a depth of 10 km inside the earth.

The compositional implications of the lunar velocity model can be explored with the aid of high-pressure laboratory measurements on lunar and terrestrial rocks. Velocity measurements have been

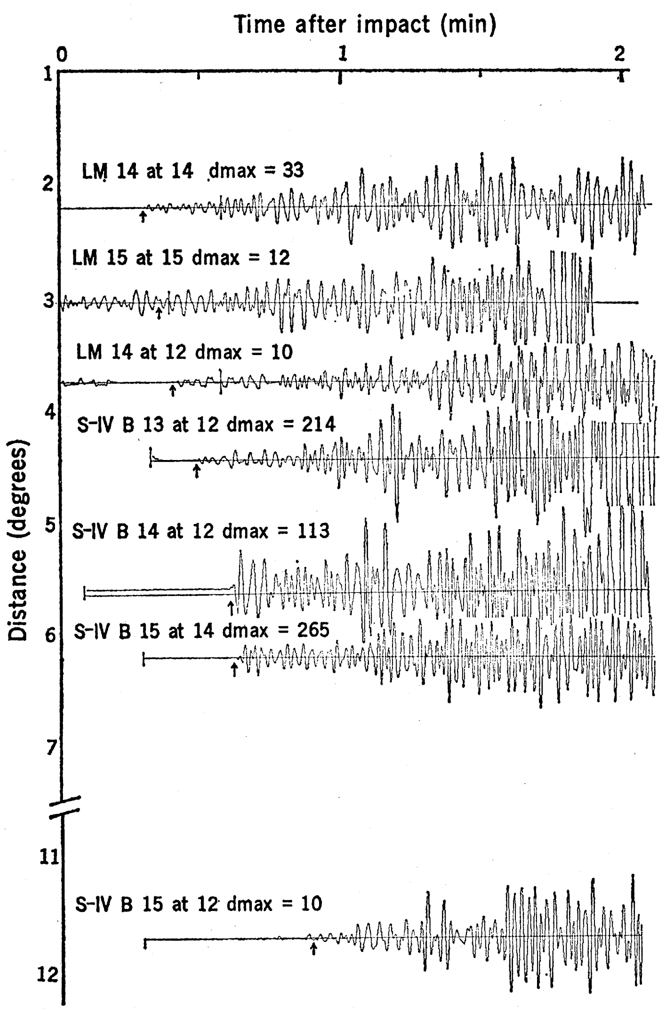

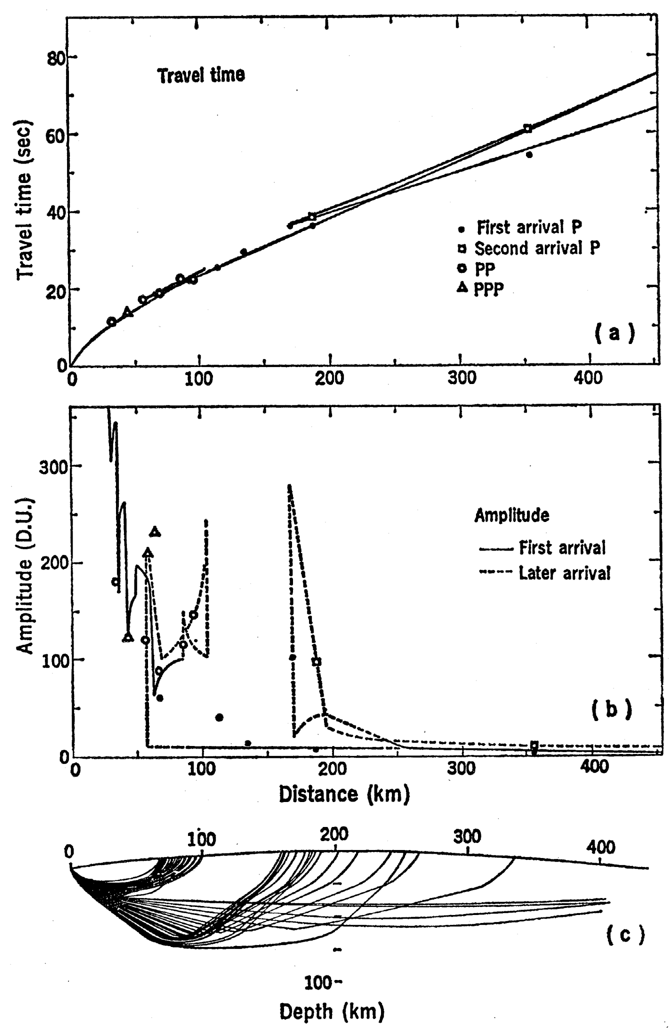

Fig. 2 (left). A composite illustration of vertical components of seismograms recorded from all artificial impacts. The notation *LM 14 at 14* means the LM-14 impact recorded at the Apollo 14 seismic station. The amplitude normalization scale is denoted by *dmax*; to yield true relative amplitudes, seismogram amplitudes must be multiplied by this factor. The distance is in degrees; 1 degree = 30.3 km. Arrows indicate the first arrivals. Note the change of character of S-IV B seismograms with distance. Fig. 3 (right). (a) Travel times and (b) amplitudes of P-wave pulses. *Second arrival P* denotes a pulse of relatively large amplitude that arrives after *P* and is associated with a travel time cusp; *PP* and *PPP* are surface-reflected phases. The lines are theoretical curves for the velocity model given in Fig. 5. Note the large amplitudes associated with travel time cusps. Digitization unit is abbreviated D.U. (c) Seismic ray paths inside the moon, for a surface source and the velocity model shown in Fig. 5. Ray crossings correspond to multiplication of travel times. The high density of the rays indicates focusing of energy and hence large amplitudes.

made for lunar soils, breccias, and igneous rocks (*5*). Regardless of composition, these rocks are characterized by very low velocities at low pressures relative to terrestrial rocks. This can be attributed to the absence of water in the lunar rocks combined with the effects of porosity and microcracks. Laboratory measurements on terrestrial igneous rocks with about 0.5 percent porosity have demonstrated this effect (*6*).

From a comparison of the laboratory data and the lunar velocity profile (Fig. 5), the following units can be identified:

1) Near the surface the extremely low seismic velocities (starting at 0.1 km/sec) are similar to those of lunar fines (soils) and broken rocks. The velocity increases very rapidly as a result of self-compaction under pressure. The exact depth to the bottom of the lunar regolith and brecciated and fractured layer cannot be determined without additional travel time data in the range $\Delta = 0.1$ to 5.0 km.

2) Below a few kilometers the measured velocities characteristic of lunar basaltic rocks fit the velocity profile to a depth of about 25 km, the observed values falling between those of rocks 10057 and 12065. The rapid increase of velocity to a depth of about 10 km can be explained by the pressure effect on dry rocks having micro- and macrocracks. Whether this layer (to 25 km) consists of a series of flows or fairly thick intrusive basalt cannot be resolved with our data. Nor is it possible to rule out other compositions or rock types that may have similar velocities in a lunar environment.

Other data support our result for the thickness of mare basalts. A model proposed by Wood *et al.* (*7*) on the basis of the densities and relative elevations of basaltic mare and "anorthositic" highlands requires 25 km of basalt in the mare for isostatic compensation to occur. The latest gravity data from Apollo *14* observations fit a model of about 20 km of basalt filling in mascon basins (*8*).

3) The second layer of the lunar crust (25 to 65 km) appears to be made of competent rock. The increase in pressure affects velocities very little (the velocity at the bottom is about 7.0 km/sec). The petrologic interpretation of the velocity curve is not simple. It can be seen in Fig. 5a that the velocities for the available lunar samples do not fit the observed curve. Thus, we must resort to laboratory data on terrestrial rocks [see (*9*) for compilations]. The

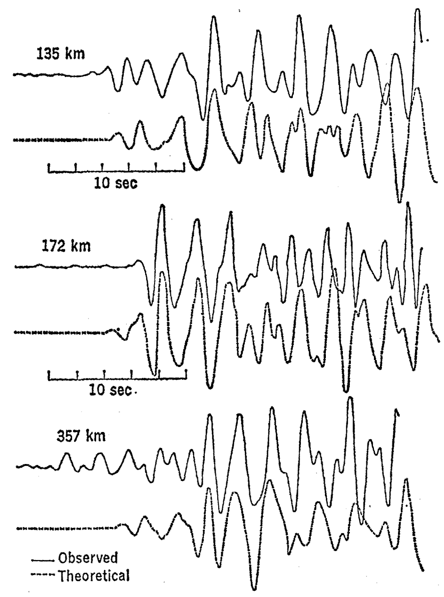

Fig. 4. Observed (solid line) and synthetic (dashed line) seismograms for three S-IV B impacts recorded at station 12. The shapes and relative amplitudes of the seismic pulses of first and later arrivals change with increasing distance. At 357 km the first two peaks of the observed seismogram are noise pulses and can be identified as such in unfiltered seismograms.

data plotted in Fig. 5b represent some possible candidates. The observed velocity curve falls in the middle of the laboratory data for gabbros and is close to the anorthosite values. The lower bound for terrestrial pyroxenite is slightly higher than the observed curve. Eclogite velocities are definitely higher than the observed velocities, and eclogite cannot be considered as a serious possibility. Petrologic evidence (*10*) as well as velocities favor a composition of anorthositic gabbro or gabbroic anorthosite, although other interpretations cannot be ruled out.

4) The discontinuity at a depth of 65 km is required to satisfy the amplitudes, travel times, and seismogram characteristics at $\Delta = 357$ km. The apparent velocity below this discontinuity increases to about 9 km/sec. Although this velocity is based on a single point and is tentative until more seismic data become available from future impacts, the discontinuity represents a major structural boundary, the interface of the lunar crust and the mantle. If the high velocity in the outer portion of the lunar mantle persists, it cannot be matched with terrestrial laboratory values.

There are four petrologically feasible candidates with relatively high seismic velocities: (i) magnesium-rich olivine (*11*); (ii) peridotite (*12*); (iii) orthopyroxene, clinopyroxine, and olivine plus spinel (*13*); and (iv) a high-pressure phase due to the transformation of anorthosite to kyanite plus grossularite plus quartz (*14*). The seismic velocities of the first three compositions are lower

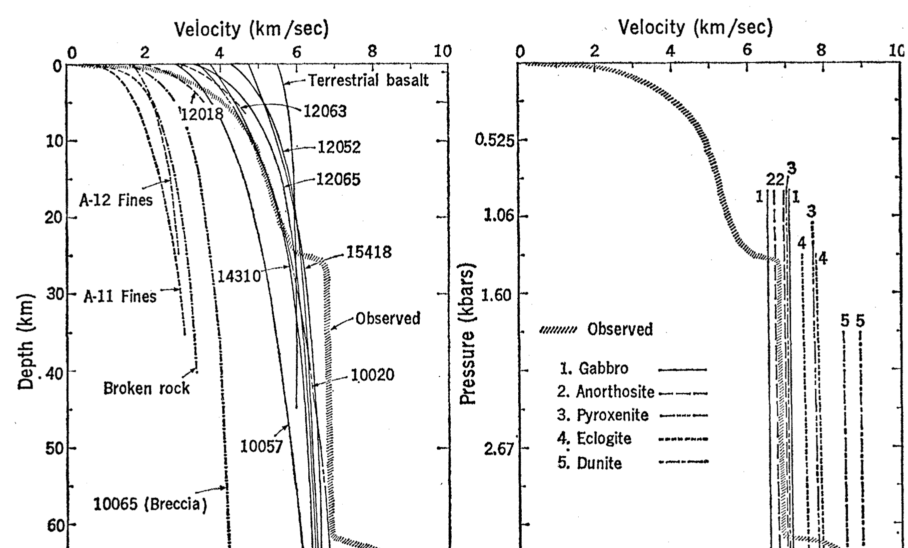

Fig. 5. Observed velocity profile (hatched lines) and velocities characteristic of lunar and terrestrial rocks measured in the laboratory as a function of pressure. (a) Lunar rocks are identified by sample numbers. The curve for terrestrial basalts is an average for basalts of the earth. (b) All the laboratory data are for terrestrial rocks. Two curves for each rock type mark the typical lower and upper boundaries of its characteristic velocities.

than the observed apparent velocity. The computed velocities for the high-pressure phase (iv) could match the observed velocities, but the nature of this composition strongly depends on minor constituents (*14*).

Any of the above petrologic models implies a differentiated lunar mantle whose composition must vary with depth to satisfy the constraints of mean density and moment of inertia. Thermal evolution calculations (*15*) imply that the crust differentiated from the outer 400 km of the moon mostly within the first 1.5×10^9 years of lunar history. The structure of the mantle and the extent of differentiation and layering cannot be determined until additional seismic data extending to greater distances (Δ) become available from future missions.

Note added in proof: Seismic signals from the Apollo 16 S-IV B impact were recently recorded at Apollo lunar stations 12, 14, and 15. The time and location of this impact were uncertain due to a loss of tracking capability. These parameters can be estimated, however, from the arrival times of P and S waves at the Apollo 12 and Apollo 14 stations. The first detectable motion at the Apollo 15 seismometer (at a distance of 1095) indicates an average velocity in the lunar mantle of at least 8 km/sec near a depth of 130 km. Whether the high-velocity (9 km/sec) zone in the uppermost portion of the mantle (reported above) is a universal feature or not cannot be determined from the new data.

The high frequencies (0.5 to 3.0 hz) of compressional and shear waves observed at station 15 from the latest impact and also from deep moonquakes indicate the absence of high attenuation, precluding widespread melting in the outer several hundred kilometers of the lunar mantle.

M. N. Toksöz, F. Press
K. Anderson, A. Dainty
Department of Earth and Planetary Sciences, Massachusetts Institute of Technology, Cambridge 02139
G. Latham, M. Ewing
J. Dorman, D. Lammlein
Lamont-Doherty Geological Observatory of Columbia University, Palisades, New York 10964
G. Sutton, F. Duennebier
University of Hawaii, Honolulu 96822
Y. Nakamura
General Dynamics Corporation, Fort Worth, Texas 76101

References and Notes

1. G. Latham, M. Ewing, J. Dorman, D. Lammlein, F. Press, N. Toksöz, G. Sutton, F. Duennebier, Y. Nakamura, *Science* **174**, 687 (1971).
2. G. Latham, M. Ewing, J. Dorman, F. Press, N. Toksöz, G. Sutton, R. Meissner, F. Duennebier, Y. Nakamura, R. Kovach, M. Yates, *ibid.* **170**, 620 (1970).
3. D. V. Helmberger, *Bull. Seismol. Soc. Amer.* **58**, 179 (1968); ——— and R. A. Wiggins, *J. Geophys. Res.* **76**, 3229 (1971).
4. R. L. Kovach, J. S. Watkins, T. Landers, *Apollo 14 Preliminary Science Report* (NASA SP-272, 1971), p. 163.
5. O. L. Anderson, C. Scholz, N. Soga, N. Warren, E. Schreiber, "Proceedings of the Apollo 11 lunar science conference," *Geochim. Cosmochim. Acta* (Suppl. 1) **2**, 1959 (1970); H. Kanamori, A. Nur, D. H. Chung, D. Wones, G. Simmons, *Science* **167**, 726 (1970); H. Kanamori, H. Mizutani, Y. Yamano, "Proceedings of the second lunar science conference," *Geochim. Cosmochim. Acta* (Suppl. 2) **2**, 2323 (1971); H. Wang, T. Todd, D. Weidner, G. Simmons, *ibid.*, p. 2327; H. Warren, E. Schreiber, C. Scholz, J. A. Morrison, P. R. Norton, M. Kumazala, O. L. Anderson, *ibid.*, p. 2345.
6. A. Nur and G. Simmons, *Earth Planet. Sci. Lett.* **7**, 183 (1969).
7. J. A. Wood, J. S. Dickey, Jr., U. B. Marvin, B. N. Powell, *Geochim. Cocmochim. Acta* (Suppl. 1) **2**, 965 (1970).
8. W. L. Sjogren, P. Gottleib, P. M. Muller, W. Wollenhaupt, *Science* **175**, 165 (1972).
9. O. L. Anderson and R. C. Lieberman, *VESIAC State-of-the-Art Report 7885-4-X* (Willow Run Laboratories, Univ. of Michigan, Ann Arbor, 1966), p. 182; F. Press, in *Handbook of Physical Constants*, S. P. Clark, Ed., (Geological Society of America, New York, 1966), Mem. 97, p. 195.
10. P. W. Gast and R. K. McConnell, Jr., in *Revised Abstracts of the Third Lunar Science Conference* (Lunar Science Institute, Houston, Tex., 1972), p. 289; A. M. Reid, J. Warner, R. S. Harmon, R. Bret, R. W. Brown, *ibid.*, p. 640; D. Walker, J. Longhi, J. F. Hays, *ibid.*, p. 770; J. A. Wood, U. B. Marvin, J. B. Reid, G. J. Tayler, J. F. Bower, B. N. Powell, J. S. Dickey, Jr., *Smithson. Astrophys. Obs. Spec. Rep. 333* (1971).
11. J. V. Smith, A. T. Anderson, R. C. Newton, E. J. Olsen, P. J. Wylie, A. V. Crewe, M. S. Isaacson, D. Johnson, "Proceedings of the Apollo 11 lunar science conference," *Geochim. Cosmochim. Acta* (Suppl. 1) **2**, 897 (1970).
12. G. M. Biggar, M. J. O'Hara, A. Peckett, "Proceedings of the second lunar science conference," *Geochim. Cosmochim. Acta* (Suppl. 2) **2**, 617 (1971).
13. D. H. Green, A. E. Ringwood, N. G. Ware, W. O. Hibberson, A. Major, E. Kiss, *ibid.*, p. 601; A. E. Ringwood and E. Essene, "Proceedings of the Apollo 11 lunar science conference," *Geochim. Cosmochim. Acta* (Suppl. 1) **2**, 769 (1970).
14. J. F. Hays, *Carnegie Inst. Washington Yearb.* **65**, 234 (1966); D. L. Anderson and R. L. Kovach, personal communication; A. L. Boettcher, *J. Petrology* **11**, 337 (1970).
15. M. N. Toksöz, S. C. Solomon, J. W. Minnear, D. Johnston, *The Moon*, in press; R. K. McConnell, Jr. and P. W. Gast, *ibid.*, in press.
16. We are grateful to Drs. B. Julian, S. Solomon, and R. Wiggins for their help and contributions during many phases of this work. Our special thanks to E. Stolper for his relentless efforts and perseverance during the analysis and interpretation of the data. Supported by NASA grants NASA-NGR 22-009-123 at Massachusetts Institute of Technology and NAS 9-5957 at Lamont-Doherty Geological Observatory.

22 February 1972

Crystal Structure of the Solid Electrolyte $(C_5H_5NH)Ag_5I_6$ at –30°C

Abstract. *The crystal structure of pyridinium hexaiodopentaargentate, $(C_5H_5NH)Ag_5I_6$, is unique among those of the halide and chalcogenide solid electrolytes in that face-sharing iodide octahedra as well as face-sharing tetrahedra and face-sharing between octahedra and tetrahedra provide the paths for silver ion transport. There are two formula units in a hexagonal cell, space group* P6/mcc (D^2_{6h}). *At $-30°C$, the lattice constants are* $a = 11.97 \pm 0.02$, $c = 7.41 \pm 0.01$ Å. *The structure has three sets of sites for the silver ions. At $-30°C$ two of these sets are apparently filled with the ten silver ions per unit cell, while the third set of tetrahedrally coordinated general positions is empty. Therefore, the conductivity at this temperature is limited by the thermal excitation of the silver ions into the empty tetrahedra.*

It has been shown (*1*) that halide and chalcogenide solid electrolytes with ionic conductivities approaching those of liquid electrolytes have cation-disordered structures and that these structures may be described as having networks of passageways resulting from the face-sharing of anion polyhedra. The number of polyhedra is usually significantly larger than the number of mobile cations.

In solid electrolytes based on a body-centered cubic arrangement of anions (for example, α-AgI) face-sharing tetrahedra only form the passageways for the mobile cations, while in those based on a face-centered cubic arrangement of anions (for example, α-Ag_2HgI_4) the passageways involve face-sharing between tetrahedra and octahedra (see *1*).

In the more complex structure of $RbAg_4I_5$ (*2*) and $[(CH_3)_4N]_2Ag_{13}I_{15}$ (*3*), the passageways are formed by face-sharing tetrahedra. Each unit cell of the former contains 56 such tetrahedra and an average of only 16 Ag^+ ions; each unit cell of the latter contains 41 tetrahedra and an average of 13 Ag^+ ions. In both cases, the passageways are interconnecting and the equilibrium distributions of Ag^+ ions over